Direct Quantitative Characterization of Polymer Brushes Obtained by Surface-Initiated ATRP on Silicon

Anne-Chantal Gouget-Laemmel, Nacim Zidelmal, Rafaela S B Soares, Nadine Barroca-Aubry, Diana Dragoe, Ludovic Costa, Bénédicte Lepoittevin, Hanène Salmi-Mani, Mohamed Mellah, Catherine Henry-De-Villeneuve, et al.

ACS APPLIED POLYMER MATERIALS

pubs.acs.org/acsapm Article

Direct Quantitative Characterization of Polymer Brushes Obtained by Surface-Initiated ATRP on Silicon

Anne-Chantal Gouget-Laemmel,* Nacim Zidelmal, Rafaela S. B. Soares, Nadine Barroca-Aubry, Diana Dragoe, Ludovic Costa, Bénédicte Lepoittevin, Hanène Salmi-Mani, Mohamed Mellah, Catherine Henry-de-Villeneuve, François Ozanam, Emmanuelle Schulz, and Philippe Roger*

Cite This: https://doi.org/10.1021/acsapm.2c01632 Read Online

ACCESS | Metrics & More | Article Recommendations | Supporting Information

ABSTRACT: With respect to the increasing need for fully characterizing surface-tethered polymer brushes, the capacity of quantitative IR-Fourier transform infrared (FTIR) spectroscopy using a multiple-internal-reflection Si prism as the attenuated total reflection (ATR) element to directly characterize the surface chemical modifications occurring during a surface-initiated controlled polymerization is investigated in the case of high-density polymer brushes. A simple two-step strategy is used involving first the covalent grafting of atom transfer radical polymerization (ATRP) initiators on a hydrogenated silicon surface and the subsequent polymerization of styrene. Three prefunctionalized surfaces designated Si-Br1, Si-Br2, and Si-Br3 are obtained by different procedures. The initiator grafting densities obtained by quantitative IR are 1.7 ± 0.3 nm^{-2} for Si-Br1, 1.5 ± 0.3 nm^{-2} for Si-Br2, and 0.9 ± 0.2 nm^{-2} for Si-Br3. After the polymerization of styrene under the same experimental conditions (grafting from without sacrificial initiators) and a careful Soxhlet rinse to remove physisorbed polymers formed in solution, almost no polymerization is observed using Si-Br1 with a value of the density in polymerized styrene units of 12 ± 2 nm^{-2}, which is probably due to the chelating effect of the amino linkers used for grafting the initiators in Si-Br1. In contrast, the densities in styrene units are 54 ± 11 nm^{-2} using Si-Br2 and 141 ± 28 nm^{-2} using Si-Br3. The degree of polymerization (DP) has been evaluated by measuring the polymer thickness (by ellipsometry and atomic force microscopy, AFM) and using a scaling law relating the latter to DP for dry polymer brushes. High DP values of 200 and 1000 are found in the case of Si-Br2 and Si-Br3, respectively. The fraction of active polymerization initiators is found to be 15−18%, independent of the initiator surface density. In contrast, polymerization kinetics appear affected by steric hindrance and conformational disorder among grafted initiators. This approach for determining surface densities of grafted initiators and grafted polymer chains and DPs is fully generalizable to any other polymer system.

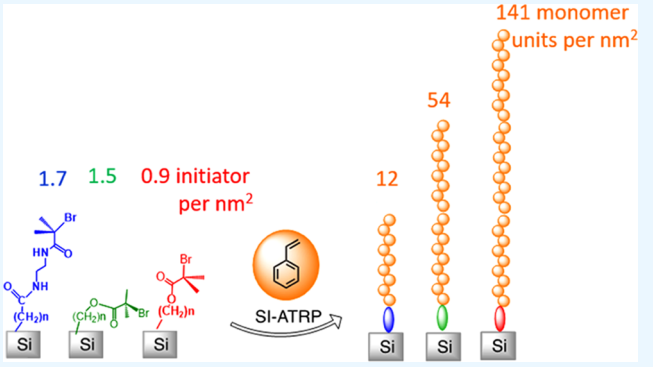

KEYWORDS: *SI-ATRP, polymerization, silicon, IR-ATR, surface functionalization*

1. INTRODUCTION

The preparation of functionalized surfaces from already existing materials is a booming activity in materials sciences as attested by the numerous recent reviews in the field.[1−5] Thus, using a very modest amount of reactant, it is possible to give properties and a very high added value to a basic and relatively inexpensive material. Often, functionalization with a monolayer is not sufficient to give the material the desired property, hence the need to use a layer of polymers to obtain sufficient thickness. The fields of application concerned are immense and diverse and depend on the type of sought properties and therefore on the type of functional entities attached at the surface of the material.[6−8] They encompass medical and public health field,[9−12] antifouling coatings in the marine environment,[13] self-cleaning day-life textiles,[14] treatment of drinking water,[15] recovery of rare metals from wastewater,[16] friction control,[17] organic electronics,[18] and supported catalysis.[19]

Many methods of surface functionalization have already been reported. In an industrial environment, dry physical methods are preferred over wet chemical grafting, as they do not require the use of solvents. In this work, a chemical route is chosen to obtain strong covalent bonds at the anchor points of the targeted chains. Two strategies of chain grafting can be

Received: September 19, 2022
Accepted: December 9, 2022

https://doi.org/10.1021/acsapm.2c01632
ACS Appl. Polym. Mater. XXXX, XXX, XXX−XXX

distinguished.[20] The grafting-to strategy allows for the attachment of chains previously synthesized and functionalized at one end. The functional groups react with the surface and establish the desired covalent bond. The other strategy is grafting-from, which permits the growth of chains after the prior implementation of the initiator on the surface. Depending on the grafting density, the chains tethered on the surface by one end adopt different conformations and different regimes can be defined.[21] At low grafting densities, "mushroom" or "pancake" conformations are described depending on the solvent quality. The coil dimension of the isolated tethered chain in good or theta solvent conditions will be similar to that of the ungrafted chains. In these conditions, the thickness of the polymer layer is of the order of $2R_G$ with R_G the radius of gyration of the free polymer chain. With increasing graft densities, chains will be obliged to stretch away from the surface forming the brush-like conformation. Polymer brushes are categorized into two groups differing in graft density: the semidilute brush and the concentrated (or high-density) brush. The crossover between the polymer chains in the semidilute regime and the concentrated regime has been observed for $\sigma \sim 0.2-0.3$ chain nm^{-2}, but for a specific system, the value may depend on the size of the pendent groups.[22,23] For each solvation regime, specific scaling laws apply between the thickness of the polymer layer, the size a of the monomer, and the chain grafting density.[20] The grafting-to methods do not reach high grafting densities to be achieved due to steric hindrance. On the other hand, the grafting-from methods, when carried out under controlled polymerization conditions, i.e., with a progressive and simultaneous growth of the chains, make it possible to obtain a high grafting density.

To achieve high chain grafting density, the grafting method has to be chosen among surface-initiated controlled radical polymerization (SI-PRC) also referred more recently to surface-initiated reversible-deactivation radical polymerization (SI-RDRP).[7,24] In this work, Surface-initiated atom transfer radical polymerization (ATRP) has been used as it is the most popular for 20 years due to its versatility and its relative ease of use.[21,25,26] Conventional ATRP typically uses a transition-metal complex as the catalyst with an alkyl halide as the initiator (R-X with X = Cl, Br, I) and various transition-metal (Mt) complexes (Mt^{n+}/L), namely, those of Cu, Fe, Ru, Ni, Os, etc., (with L: ligand) have been employed as catalysts for ATRP. In an SI-ATRP process, the initiator is grafted onto the surface. Then, the polymerization is conducted in a controlled manner either in the presence of untethered sacrificial initiator or in the absence of untethered sacrificial initiator but with 5−25 mol % of deactivator (Mt^{n+1}/L) with respect to the activator (Mt^{n+}/L).[27,28] Since the initial ATRP works, many attempts have been made to lower or even suppress the amount of catalyst (often copper) used in ATRP. Among them are the metal-free ATRP[29,30] or the externally controlled ATRP[31] such as eATRP[32−34] or photoATRP[35−37] being controlled by electrical current or light, respectively.

In the SI-ATRP modification, the main drawbacks are the difficulty of analyzing the length of the polymer chains grafted onto the surface as well as the grafting density. Using the above-mentioned scaling laws, measurements of polymer thickness in dry and solvated states can give access to the degree of polymerization and grafting density.[38−40] However, the polymer coatings are analyzed by tedious or indirect methods. The grafted polymer chains can indeed be detached from the surface for analysis, after either destruction of the substrate or chain release by hydrolysis.[41] Another method is the analysis of the polymers obtained in solution, by the activation of a sacrificial initiator introduced into the reaction medium. In that case, it must be assumed that similar mechanism and kinetics take place for the polymerization both in solution and from the surface. This method is usually considered a good check for polymerization control. In the absence of untethered initiator, another possibility to maintain the controlled polymerization is to add a sufficient concentration of deactivator.[27] The advantage of this method is the absence of free polymers produced in solution, which could pollute the surface by adhesion. However, the degree of polymerization and chain grafting density have then to be directly determined. A new method requiring characterization of the polymer layer in the dry state only is presented here for that purpose.

The approach consists in performing polymerization on crystalline silicon prisms and using quantitative IR spectroscopy in attenuated total reflection (ATR) geometry. Then, with a single measurement of the polymer layer thickness (using ellipsometry or AFM), the grafting density, the length of the polymer chains, their DP, and the fraction of active tethered initiators can be directly obtained. Working with a silicon prism providing multiple internal reflections (typically ~20 reflections) gives the requested sensitivity.[42−45] Silicon prisms are commercially available and many (electro)chemical strategies have been developed to graft organic moieties, such as usual initiators, via Si−C or Si−O−C covalent linkages.[46−48] Finally, the IR configuration is well known at the prism surface,[49] allowing for quantitatively analyzing the IR bands and determining the density and the orientation of the molecules grafted to the prism.[50] Molecular densities as low as ~0.15 nm^{-2} have been determined, corresponding to ~0.1 equiv of one monolayer, providing the requested sensitivity to determine practical initiator densities.[51]

Herein, the method is presented for the case study of high-density polystyrene brushes synthesized using the SI-ATRP procedure after initial grafting of the initiator onto the prism surface. Three different routes of introduction of this initiator via Si−C covalent bonds have been developed to modulate the density of grafted initiators and assess the corresponding impact on the styrene polymerization efficiency. The polymerization of styrene has been conducted in classical ATRP conditions, in the absence of untethered sacrificial initiator. Kinetics studies assessing the control of the polymerization process on silicon surface have been conducted in the initial work of Matyjaszewski et al.[27] For polymerization in solution, ethyl 2-bromoisobutyrate has been used as the initiator.[52,53] In such conditions, the polymerization was well controlled with first-order kinetics, a linear increase of M_n with conversion and molar mass dispersities $Đ$ in the range 1.07−1.10.[54]

2. RESULTS AND DISCUSSION

2.1. Grafting of ATRP Initiator via Three Strategies. In the first approach displayed in Figure 1A, well-defined carboxydecyl-terminated silicon(111) surfaces have been chosen as the starting state for the step-by-step covalent grafting of the polymerization initiator for several reasons. First, they are obtained by photochemical hydrosilylation of 10-undecylenic acid on hydrogenated silicon surfaces, leading to a robust attachment of the alkyl chains via covalent Si−C bonds.[50] Rather high density of acid chains can be achieved, typically between 2 and 3 acid chains·nm^{-2}, which is a key

https://doi.org/10.1021/acsapm.2c01632
ACS Appl. Polym. Mater. XXXX, XXX, XXX−XXX

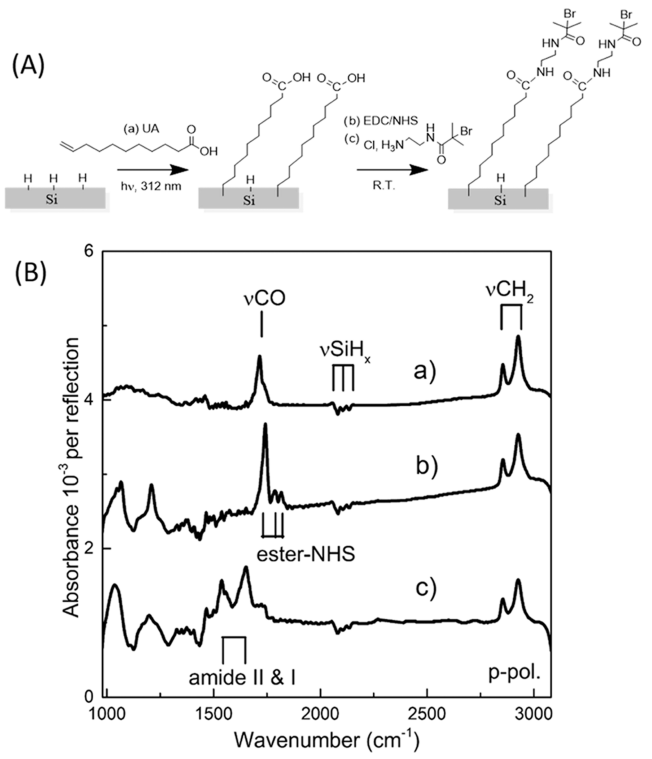

Figure 1. Multistep chemical modification of crystalline silicon Si(111) surface (A) and the corresponding ATR-FTIR spectra in p-polarization after (B): the photochemical hydrosilylation of 10-undecylenic acid on the etched SiH_x surface leading to the carboxy-terminated surface, Si-acid (a); the activation of the acid functions via EDC/NHS (b); the amide bond formation by coupling the ester-NHS functions with initiator 1 in aqueous medium leading to Si-Br1 (c). Absorbance is computed with respect to the hydrogenated Si(111) surfaces.

parameter to obtain brush-like polymers on the surface.[21] Finally, the terminal carboxyl functions can be modified with amino linkers in mild conditions using the well-known 1-ethyl-3-(3-dimethylaminopropyl)carbodiimide/*N*-hydroxysuccinimide (EDC/NHS) coupling strategy.[55−58] In this case, an aminoethyl-substituted compound bearing an α-bromoisobutyryl moiety has been proposed as a polymerization initiator (initiator 1) to be grafted on the surface via amide bonds.[6,59] Its synthesis as a hydrochloride salt has been realized in three steps as described in the Experimental Section.[60]

To characterize the immobilization of the initiator 1 directly on the silicon surface, ATR-FTIR spectroscopy has been performed using the modified silicon prism as the ATR element. Figure 1B represents the IR spectra of the silicon surface after each chemical modification: 10-undecylenic acid grafting (a), EDC/NHS activation (b), and amide bond formation with initiator 1 (c). In either case, the reference spectra are that of the freshly etched Si(111) surface (abbreviated as SiH_x). Focusing on the 1500−1900 cm^{-1} spectral range, the carbonyl stretching mode νCO of the acid-terminated surface is clearly seen at 1715 cm^{-1} and the triplet band at ∼1743 cm^{-1} is characteristic of the νCO modes of the ester-NHS function of the activated surface.

After reaction of the ester-NHS groups with initiator 1, spectrum (c) reveals the complete disappearance of the triplet band and the presence of the two amide bands at 1650 and 1535 cm^{-1}, confirming the success of the initiator grafting. The carbonyl peak is still present at a higher wavelength of ∼1727 cm^{-1} suggesting unreacted acid or partial hydrolysis of ester-NHS functions during the aminolysis. To determine the yield of the chemical modification of the grafted carboxydecyl chains, we have developed quantitative tools from the integrated absorbance of the carbonyl peaks measured for the p- and s-polarization of the IR beam.[50,61] Briefly, an IR calibration using similar molecules (decanoic acid in dodecane and *N*-succinimidyl palmitate in tetrahydrofuran, THF) is performed at different concentrations to determine the absorption cross-section of the carbonyl modes of the carboxylic acid and the ester-NHS functions as explained in supporting information, Section S-I. By comparing the integrated areas of characteristic peaks with the corresponding ones of the grafted molecules, two characteristic quantities $N_{//}$ and $N_{\perp}$ can be computed. They are equivalent to a surface concentration of molecules corresponding to the projection of the dynamic dipole of the considered mode on the surface and its normal, respectively. The actual areal density of the carbonyl functions is deduced from the sum $N_{//} + N_{\perp}$, and the number of grafted acid and ester-NHS chains per nm^2 can this way be calculated. Table S1 summarizes the integrated absorbance of the carbonyl peaks in p- and s-polarization of the various modified surfaces, and Table 1 shows the corresponding grafting density. Furthermore, an independent IR calibration of dodecane has been achieved to determine the surface concentration of methylene units in the grafted chains through the analysis of the νCH_2 band chains. On carboxydecyl layers, this calibration essentially yields the same results as that based on the analysis of the νC=O band. A density of 2.3 ± 0.4 grafted chains per nm^2 for the carboxydecyl-terminated Si(111) monolayer is found, whereas a density of 2 ± 0.4 ester-NHS chains per nm^2 is obtained, which corresponds to an activation yield of ∼85%. In the case of the Si-Br1 surface, a residual amount of ∼0.6 ± 0.1 acid chains per nm^2 is calculated, given a total amidation yield of ∼70% with 1.7 ± 0.3 bromoisobutyryl-terminated chains per nm^{-2}. It means that ∼20% of the surface Si atoms are linked to

Table 1. Molecular Density *N* (in nm^{-2}) at Various Modification Stages of Si(111) Surfaces, According to Strategies 1, 2, and 3

	starting surface (from νCO or $\nu_s CH_2$)		initiator-grafted surface (from νCO)	polymerized surface (number of styrene units from νCH_{aro})
strategy 1	Si-acid (from vCO/$\nu_s CH_2$)	Si-ester NHS (from vCO)	Si-Br1	Si-PS1
	2.3 ± 0.4/2.6 ± 0.5	2 ± 0. 4	1.7 ± 0.3[a]	11.6 ± 2.2
strategy 2	Si-ester (from $\nu_s CH_2$)		Si-Br2	Si-PS2
	1.53 ± 0.3		1.5 ± 0.3	54.2 ± 11
strategy 3	hydrogenated surface		Si-Br3	Si-PS3
	no grafted molecule		0.9 ± 0.2	141 ± 28

[a]Based on the determination of the surface concentration of residual acid groups.

https://doi.org/10.1021/acsapm.2c01632
ACS Appl. Polym. Mater. XXXX, XXX, XXX−XXX

an initiator-terminated chain, a figure to be compared to the grafting of ∼50% of the surface Si atoms in the most dense alkyl layers.[62] The water contact angle of the three surfaces was also measured: it rises from 61 ± 1° for the acid surface to 67 and 74 ± 1° after the NHS activation and amidation reaction, respectively, confirming the grafting of nonpolar terminal groups on the silicon surface.

As a second strategy, the commercially available α-bromoisobutyryl bromide (initiator 2) has been immobilized on the Si surface via an ester linkage as depicted in Figure 2A.

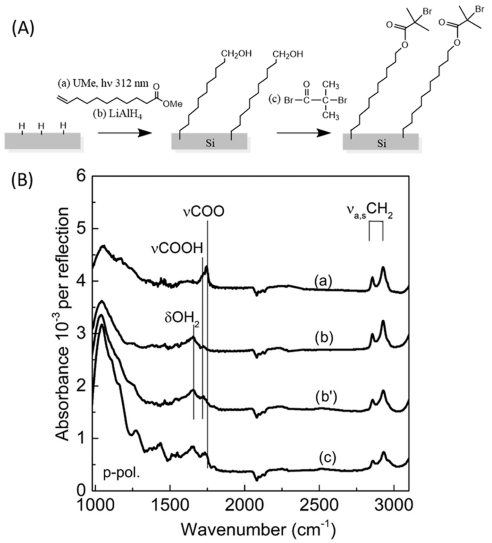

Figure 2. Multistep strategy for the attachment of α-bromoisobutyryl initiator (initiator 2) via ester bonds (A) and their corresponding ATR-FTIR spectra in p-polarization at various stages of the attachment procedure (B): photochemical hydrosilylation of methyl 10-undecenoate on the SiH_x surface, Si-ester (a); reduction of the ester functions with $LiAlH_4$ (b) followed by a vacuum drying at 80 °C, Si-OH (b'); esterification of the hydroxyl functions with α-bromoisobutyryle bromide, Si-Br2 (c). Absorbance is computed with respect to the hydrogenated SiH_x surface.

Similar strategies have proven to be efficient for the growth of brush-like polymer chains by SI-ATRP on various substrates like silicon,[27,63,64] polymers,[65,66] and nanoparticles.[7,24] The surface modification involves three steps. The photochemical hydrosilylation of methyl-10-undecenoate on SiH_x leads to the formation of the ester-decyl-terminated monolayer Si-ester. Then, the ester groups are reduced in the presence of $LiAlH_4$ to form the hydroxyl-terminated surface Si-OH; the latter is finally esterified by reaction with initiator 2. Figure 2B shows the IR-ATR spectra of the three different monolayers. From spectrum (a), a broad peak with a maximum at 1747 cm^{-1} is attributed to the stretching mode of the ester function together with a shoulder at 1724 cm^{-1} related to the νCO mode of the carboxylic acid, suggesting the partial hydrolysis of the ester groups into acid groups. Since the two carboxyl and ester peaks overlap, their fitting is very sensitive to the width of their bands. The quantification has therefore been focused on the quantification of the $\nu_s CH_2$ mode from the alkyl chain to extract an areal density of ∼1.53 ± 0.3 grafted chains per nm^2. After reduction with $LiAlH_4$, spectrum (b) reveals the complete disappearance of the acid and ester functions and the appearance of a broad peak at 1653 cm^{-1} maybe due to entrapped water molecules (δ_{H2O} scissor mode) interacting by hydrogen bonding on the hydroxylated surface. Heating at 80 °C under vacuum does not remove the presence of this peak but favors the oxidation of the surface as unveiled on the IR spectrum (b') with a broad peak at 1040 cm^{-1} corresponding to the silicon oxide vibrations. In the last spectrum (c), the peak related to the νCO of the ester becomes again visible and shifted to 1739 cm^{-1}, attesting to the successful attachment of initiator 2. The surface Si-Br2 is further oxidized. The oxide thickness can be estimated from the intensity of the band at 1040 cm^{-1} related to the transverse optical phonon vibration in s-polarization (in this case, 2.3 mAbs, data not shown). As 1 mAbs corresponds to a thickness of ∼1.5 Å, a 3.4 Å-thick oxide film is estimated.[67] To avoid interference with the residual peak at 1720 cm^{-1} present after the vacuum heating treatment, the quantitative analysis of the ester peak was performed on spectrum (c) by taking the spectrum (b') as the reference spectrum (Figure S6). For the quantification of grafting density of the Si-Br2 surface, IR calibration of undecenyl isobutyrate (initiator 3) has been realized as explained above. A density of 1.49 ± 0.3 initiator-terminated chains per nm^{-2} is calculated, yielding to a quantitative conversion of the initial ester chains within the accuracy of the molecular density determination. From ellipsometry analysis, the thickness of the layer amounts to 1.4 nm, close to the calculated thickness of 1.48 nm with a tilt angle of 30−35° (determined by Chemdraw software). However, the actual geometry of the chains appears to depart from this ideal picture, in which the orientation of the C═O bond is expected to be ∼60° off the surface normal. Identifying the C═O bond direction to the orientation of the dynamic dipole of the stretching C═O bond, the corresponding average orientation of the C═O can be experimentally determined as $\tan^{-1}[(N_{//}/N_{\perp})^{1/2}]$, which yields a value of ∼38°. Infrared data therefore suggest the presence of conformational defects like gauche conformers in the grafted layer. A possible explanation of this departure from an ideal configuration can be thought of as arising from the intermediate SiOH surface. The presence of hydroxyl termination could induce some chain pairing through the mediation of water molecules, to favor the buildup of an energetically favorable hydrogen-bond network. The presence of strongly bound water molecules evidenced in the infrared spectra supports this hypothesis. The induced chain pairing favors the presence of gauche conformation in typically half of the grafted chains. By assuming that this conformation does not change in the final esterification step, an average orientation of the C═O bonds of ∼30° with respect to the surface normal is expected, in typical agreement with the low value experimentally determined. In any case, infrared data reveal the presence of a significant conformational disorder on top of the grafted layer.

The last strategy consists in grating initiator 3 (an alkenyl chain terminated with a bromoisobutyrate head) on a hydrogenated silicon surface. Initiator 3 was synthesized in one step with excellent yield from the esterification of 10-undecenol with α-bromoisobutyryl bromide (initiator 2).[57] The hydrosilylation reaction was performed thermally to avoid competitive homolytic C−Br bond cleavage when using UV irradiation. Figure 3 represents the ATR-IR spectrum of initiator 3 grafted on Si(111), Si-Br3. The presence of the stretching modes of the alkyl chains at 2860 and 2925 cm^{-1} together with their bending mode at 1465 cm^{-1} and the stretching mode of the ester link at 1735 cm^{-1} confirms the

https://doi.org/10.1021/acsapm.2c01632
ACS Appl. Polym. Mater. XXXX, XXX, XXX−XXX

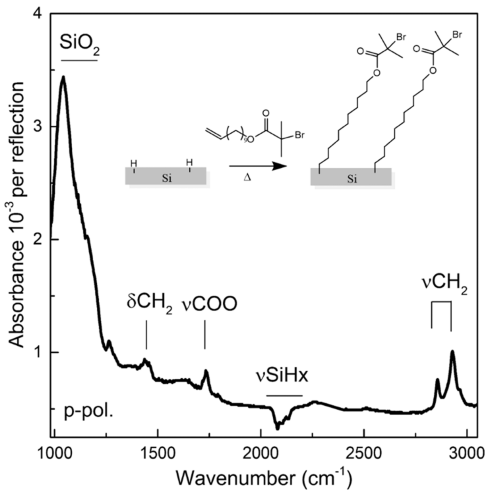

Figure 3. ATR-FTIR spectrum in p-polarization after the direct thermal hydrosilylation of initiator 3 on the SiH_x surface. Absorbance is computed with respect to the hydrogenated SiH_x surface.

grafting of initiator 3 on the surface. The stretching and the bending mode of the methyl groups are also observed at 2965 and 1265 cm^{-1}, respectively. In parallel, the surface Si-Br3 is quite oxidized with an oxide peak absorbance of 2.6 mAbs in s-polarization at ~1050 cm^{-1}, corresponding to an equivalent oxide thickness of 3.9 Å.

For the quantification of the ester peak, an IR calibration of initiator 3 has been realized in $CDCl_3$ at various concentrations (cf. Section S-I). A density close to 0.9 ± 0.2 initiator-terminated chains per nm^2 is calculated. This value is low (3 times lower than that of closely packed alkyl layers on Si(111) and significantly lower than the value obtained using the first strategy). The successful grafting was also evidenced by X-ray photoelectron spectroscopy (XPS). The C 1s core-level spectrum (Figure 4A) is separated into four main contributions at 284.3 eV related to a carbon linked to Si (C−Si), at 285.1 eV attributed to sp3 carbon only linked to C or H atoms (Csp3), at 286.6 eV to carbon linked to bromine or the terminal carbon of an alkyl chain linked to the oxygen atom from an ester group, and finally at 289.1 eV to the carbon of an ester function (C-ester). From the quantitative analysis of the normalized areas of these contributions (Table S4), the ratio of Csp3/C-ester can be determined and is perfectly equal to 11, as expected for surface species $Si-CH_2-(CH_2)_9-CH_2-OOCC-(CH_3)_2Br$. However, the ratio C-ester/C−Si is twice smaller as expected (~0.47 instead of 1). Part of this low value can actually arise from the attenuation of the photoemitted electrons by the surface organic layer since the Si−C bonds are located at the bottom of the layer, whereas ester groups are located at the top. On the basis of the attenuation of a $C_{16}H_{33}$ layer,[68] a transmission coefficient of ~0.67 can be estimated for the organic layer, which might account for the about half of the discrepancy with the expected value of the Si−C contribution to the C 1s band. Another possible origin for this discrepancy can be paralleled with the value of the C−Br, C−O/C-ester contribution ratio, which is equal to 2.5 instead of 2. Since the surface is strongly oxidized with a characteristic contribution at ~103.0 eV in the Si 2p XPS spectrum (Figure S7), it can be suggested that part of the initiator 3 molecules have reacted with surface SiOH species generated during the reaction upon surface oxidation by residual water. Even though the detailed mechanism remains to be clarified, the generation of some $Si-O-(CH_2)_{11}-OOCC(CH_3)_2Br$ species at the surface is consistent with a decrease in the expected Si−C contribution and an increase of that of C−Br, C−O to the C 1s band. To put in another way, some grafting may also occur via Si−O−C linkage. The overlap of the various contributions to the C 1s band makes uncertain the accurate determination of the respective proportions of the chains grafted through a Si−C bond to that grafted through a Si−O−C bond. The data are consistent with a proportion of molecules grafted through Si−O−C bonds up to 50%. Finally, the Br 3d core-level spectrum is fitted using two spin−orbit splitting doublet located at ~70.5 eV (Br $3d_{5/2}$) and ~71.4 eV (Br $3d_{3/2}$), attributed to Br−C bounds and a second at ~69.4 eV (Br $3d_{5/2}$) and ~70.4 eV (Br $3d_{3/2}$) given by negatively charged Br, which forms during exposure to the X-ray beam (Figure 4B).[69] From the

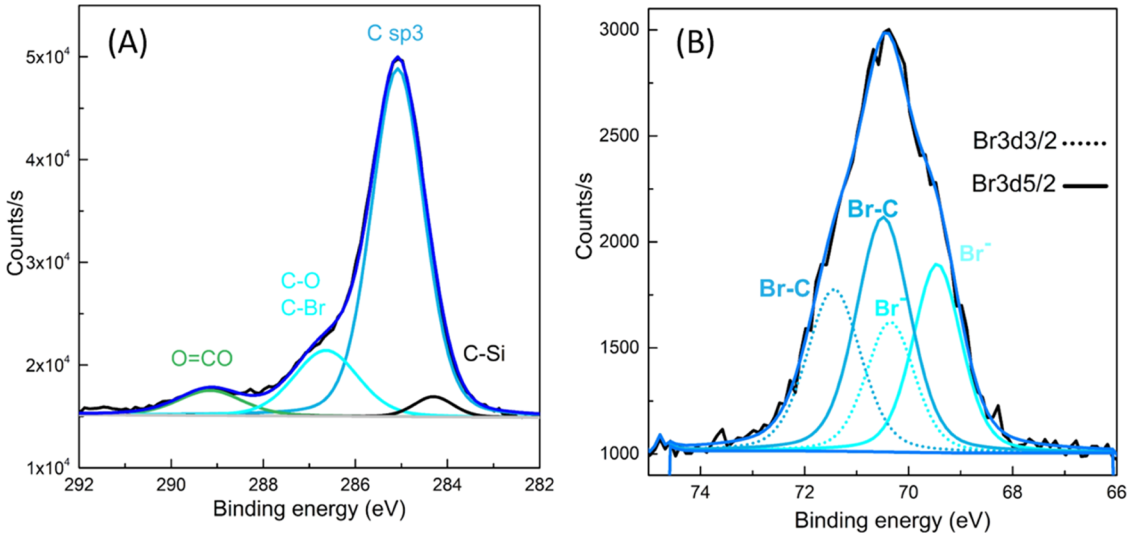

Figure 4. XPS spectra of the direct thermal hydrosilylation of initiator 3 on SiH_x surface: in the C 1s (A) and Br 3d (B) regions. The normalized areas of the contributions to C 1s are 3.2% for O═C−O, 8.2% for C−Br/C−O, 35.3% for Csp3, and 1.5% for Si−C (see Section S-II and Table S4).

https://doi.org/10.1021/acsapm.2c01632
ACS Appl. Polym. Mater. XXXX, XXX, XXX−XXX

ellipsometry analysis, the thickness of the film is evaluated to 1.7 nm, a much higher value than those obtained in the indirect strategy for the preparation of Si-Br1 and Si-Br2. However, this value is close to those reported for monolayers with such types of initiators.[24,70] The contact angle of Si-Br3 is 75 ± 1°, which is close to the value of Si-Br1. Noteworthy, the infrared data give an average orientation of the C═O bond (determined from the $N_{//}/N_{\perp}$ ratio) close to 53° off the surface normal. This is compatible with a geometry of the grafted chains close to an ideal all-trans conformation (which would yield a value of ∼60°), regardless of the attachment to the surface achieved through Si−C or Si−O−C bonds.

2.2. SI-ATRP of Styrene. For the polymerization of styrene on the surface, no sacrificial initiator is needed but an excess of deactivator $CuBr_2$ was added with (monomer)/(CuBr)/($CuBr_2$)(PMDETA) = 100/1/1/1.2 molar ratio. The same polymerization conditions were used on the three types of initiator functionalized surfaces: Si-Br1 and Si-Br2 afforded from the two-step strategy using acid or ester-terminated monolayer as primary anchoring layer, respectively, and Si-Br3 obtained by the direct grafting of initiator 3 on the pristine SiH_x surface. A final rinse using a Soxhlet in dichloromethane for 24 h is mandatory to remove physisorbed polystyrene formed in solution. Figure 5 displays the ATR-FTIR spectra in

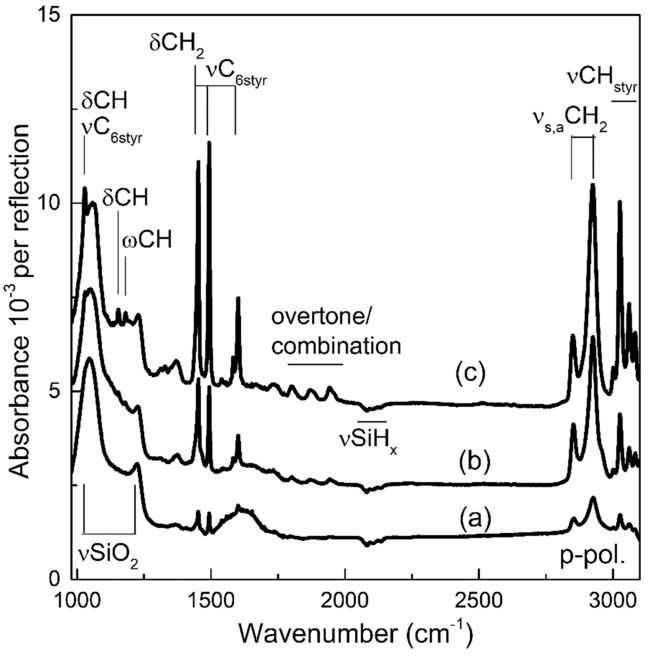

Figure 5. ATR-FTIR spectra in p-polarization of Si(111) surfaces modified with polystyrene chains, Si-PS1 (spectrum a) starting from Si-Br1, Si-PS2 (spectrum b) starting from Si-Br2, and Si-PS3 (spectrum c) starting from Si-Br3. Absorbance is computed with respect to the hydrogenated SiH_x surfaces.

p-polarization of three polystyrene-modified Si surfaces, (a) Si-PS1 (b) Si-PS2, and (c) Si-PS3 obtained from Si-Br1, Si-Br2, and Si-Br3, respectively. In either case, the main peaks related to the polystyrene formation are observed: the stretching modes of the C−H from the benzene ring between 3003 and 3084 cm^{-1}, the strong IR active ring stretch vibrations for which the CH group moves essentially as a unit at 1604 cm^{-1} (quadrant stretch mode), 1492 cm^{-1} (semicircle stretch mode); at 1453 cm^{-1} the observed band results from the contribution of a semicircle stretch mode of the benzene ring and that of the in-plane deformation mode of the methylene units of the polymer chain.[71,72] Other less-intense vibrations related to the polystyrene chains are revealed in spectra (b) and (c): the symmetric and asymmetric stretching νCH_2 modes of the methylene chains at 2850 and 2924 cm^{-1}, the overtone/combination bands of the monosubstituted benzene ring in the 1800−1945 cm^{-1} range. Further contributions at 1330 cm^{-1} (sextant stretch mode of the ring mixed with a CH in-plane bending mode) and 1311 cm^{-1} (centrosymmetric CH in-plane bending mode) are also found. By comparing spectra (b) and (c), the IR band intensities are much larger in the case of the Si-Br3 surface (spectrum c) than in the case of the Si-Br2 surface (spectrum b), by a factor of 2.5−2.8 for the two sharp peaks at 1455 and 1493 cm^{-1}. New peaks are also revealed at 1028, 1155, and 1180 cm^{-1}, a mode mixing ring quadrant stretch and in-plane CH bending, the in-plane bending mode of the CH group in para position, and a combination band involving out-of-plane CH deformation modes, respectively. On the contrary, the two bands related to Si−O−Si vibrations are rather similar in all spectra, arising from an oxide layer whose thickness is estimated to be close to ca. 6.5−7.5 Å. This strong oxidation may be induced by the presence of the copper metal at 100 °C on the silicon surface.[73]

From this analysis, the styrene polymerization seems to be much more efficient when starting from Si-Br3, than from Si-Br2 and even more than from Si-Br1. At first glance, this result may be related to the different densities of the grafted initiator chains (0.9 nm^{-2} for Si-Br3 vs 1.5 nm^{-2} for Si-Br2 and 1.7 nm^{-2} for Si-Br1), a lower steric hindrance favoring the growth of PS chains on the surface. In either case, the initiator density is much higher than the density of brush polymers typically up to 0.4 nm^{-2}.[22,38] Other factors are also plausible. For instance, it has been seen that the chain conformation is more ordered on SiBr3 than on SiBr2; the conformational disorder on SiBr2 could be less favorable to polymerization. Moreover, though the density of grafted initiator is rather similar between Si-Br1 and Si-Br2, the polymerization is inefficient on the Si-Br1 surface. Indeed, a slight increase of the two $\nu_{s,a}CH_2$ bands corresponding to the methylene (CH_2−CH_2) groups is visible when the spectrum of the Si-Br1 surface is taken as a reference (cf. Figure S8). Their intensities are quite low (<0.5 mAbs) compared to those of the carbonyl and alkyl peaks, suggesting the growth of a few polystyrene chains at the surface corresponding to a surface concentration in styrene units of a few monolayers only. Although many optimizations were attempted (i.e., increase of the reaction time, temperature change, use of various ligands···), styrene cannot be efficiently polymerized by SI-ATRP on Si-Br1 surface. A possible explanation is that the two nitrogen atoms present in Si-Br1 may complex with the Cu catalyst inhibiting the ATRP polymerization.

The morphology of Si-PS2 and Si-PS3 polystyrene layers were then investigated by AFM (Figure 6) and their thickness was measured by locally removing the organic layer. In both cases, the images reveal a homogeneous coverage of the surface by a dense and homogeneous layer (Figure 6a,b) but with different thicknesses: ∼11 nm for the Si-PS2 layer and ∼29 nm for Si-PS3 (Figure 6c,d). These values are in good agreement with those deduced from ellipsometry measurements (9 nm for Si-PS2 and 27 nm for Si-PS3). They are furthermore consistent with the relative intensity of the polystyrene IR bands

https://doi.org/10.1021/acsapm.2c01632
ACS Appl. Polym. Mater. XXXX, XXX, XXX−XXX

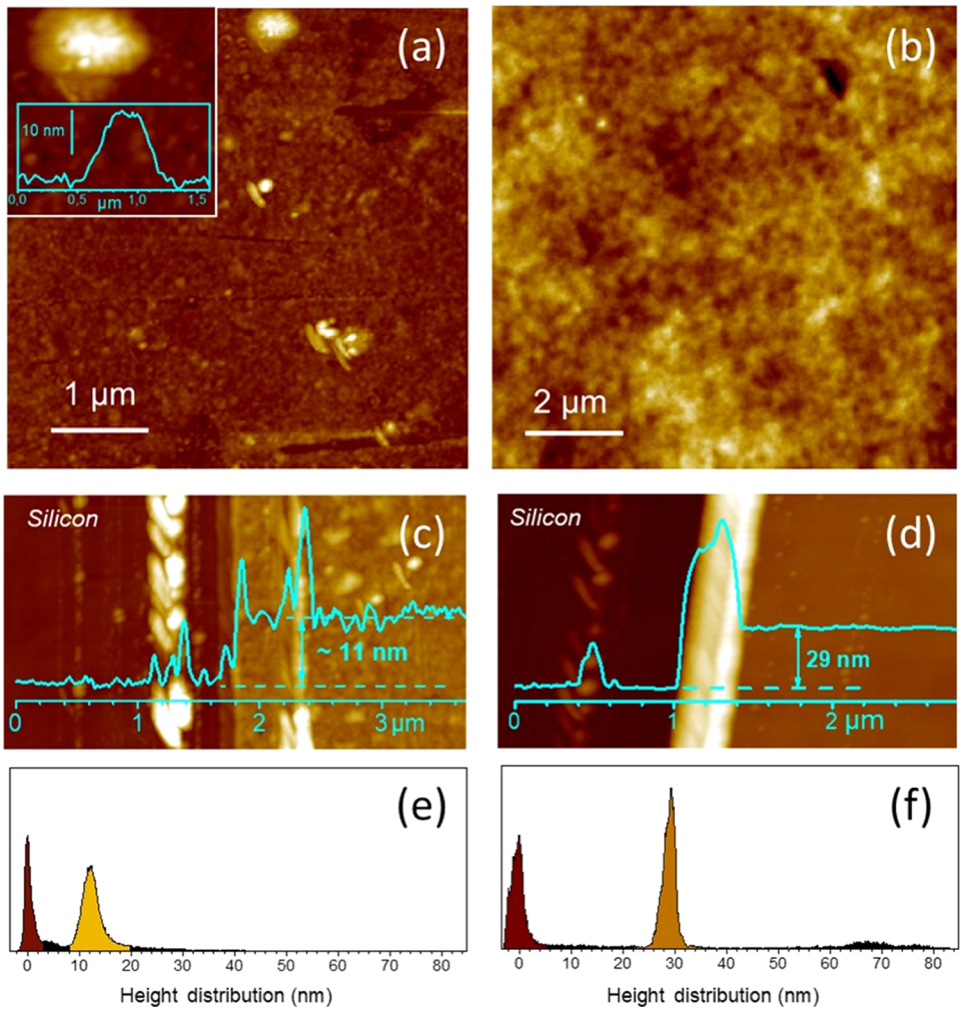

Figure 6. AFM characterization of the Si-PS2 (left column) and Si-PS3 (right column) polystyrene layers. (a, b) Top-view images of the layers. The inset in (a) shows a higher-magnification one of the 3D aggregate found atop the layer. Note its characteristic ∼15 nm height corresponding to twice the thickness of the layer and its structure corresponding to an assembly of smaller structures. (c, d) Top-view images and cross sections at the frontier between the silicon substrate and the polystyrene layer. (e, f) Height distributions corresponding to images (e) and (f) give the mean thickness of the layers: ∼11 nm for Si-PS2 and ∼29 nm for Si-PS3.

corresponding to these two layers (greater intensity of the IR bands for the thicker Si-PS3 layer). In the case of the Si-PS2 layer, the images also reveal the presence of a low density ($\sim 10^8/cm^2$) of three-dimensional (3D) aggregates with characteristic sizes (∼15 nm height and a few hundred nm width) atop the layers (Figure 6a, inset). These aggregates look like assemblies of smaller structures with size comparable to those found in the underneath layer. Their height, about twice as large as the layer thickness, suggests they might be also polystyrene chains aggregated atop the layer. From their volume (assuming a spheroid shape) and their density, the amount of matter corresponding to these aggregates may be roughly calculated. An equivalent thickness of ca. 3−4 nm is found. Such aggregates are not observed for the Si-PS3 layer.

2.3. Quantification of the Polymer Brushes. To get quantitative information about the number of grafted PS chains, an IR calibration of polystyrene in solution was performed to convert the absorbance of the peaks characteristic of PS into the areal density of the PS chains. For this, ATR-FTIR spectra of polystyrene were measured at different concentrations in $CDCl_3$ in s-polarization as presented in Figure S9 and the magnitude of the sharp peak at 1493 cm^{-1} is used for determining the areal density of styrene units, as detailed in Sec S-I and S-III. From these results, the surface concentration of styrene units was derived: 11.6 ± 2.2 nm^2 for Si-PS1, 54.2 ± 11 nm^{-2} for Si-PS2, and 141 ± 28 nm^{-2} for Si-PS3. To obtain the density of grafted PS chains, the degree of polymerization (DP) is needed. This piece of information can be derived from the thickness of the polymer layer. Polymer chains densely grafted at a surface (polymer brushes) usually adopt a collapsed and less organized structure where the chains are not so well oriented and fully extended, in contrast to ordered monolayers of grafted molecules such as that of the SiBr3 surface. Considering a brush without solvent (bulk state), the thickness L of the polymer brush only depends on DP and obeys a scaling law $L \sim DP^{2/3}$.[20] In this case, the thickness of the polymer brushes is normalized to the average distance a between two monomer units along a polystyrene chain (∼0.25 nm), leading the following scaling law $L/a = DP^{2/3}$. Starting from a polymer thickness of 8.6 nm (SiPS2) or 26.3 nm (SiPS3), a DP of ∼200 (SiPS2) or ∼1000 (SiPS3) is derived from the scaling law. This yields a fraction of active initiators of 18 and 15% for SiPS2 and SiPS3, respectively. We did not attempt a similar analysis for SiPS1 since, as mentioned

https://doi.org/10.1021/acsapm.2c01632
ACS Appl. Polym. Mater. XXXX, XXX, XXX−XXX

above, the polymerization efficiency is poor for this configuration.

The initiation efficiency then appears similar for SiPS2 and SiPS3, in spite of the distinct features of the SiBr2 and SiBr3 surfaces in terms of initiator areal density and conformational ordering. On the contrary, the conversion obtained by starting from SiBr3 appears significantly higher than that obtained when starting from SiBr2, as reflected by the differences in the areal density of styrene units measured by infrared spectroscopy. Since in either case polymerization is performed in the same experimental conditions, this difference reveals that polymerization kinetics are hindered to a larger extent when starting from SiBr2 than when starting from SiBr3. This kinetic limitation likely comes from steric hindrance (higher areal concentration of active initiators for SiPS2), or from the conformational disorder of the SiBr2 surface, as revealed by infrared spectroscopy, or from both origins. Experiments using mixed layers obtained by grafting of 10-undecen-1-yl-2-bromo-2-methylpropionate diluted in 1-decene at variable concentrations are under consideration for addressing this issue.

These results point to the fact that differences in the density or conformation of tethered initiators at the surface do have consequences in terms of polymerization efficiency. Such differences would not appear in the usual approach where the bulk polymers resulting from the addition of untethered initiators are analyzed. Therefore, a method such as that proposed here offers a much more relevant and reliable picture of the tethered polymer. In addition, the fraction of active initiators is also obtained.

3. CONCLUSIONS

For the first time, ATR-FTIR quantification together with AFM imaging offers an alternative to the indirect classical methods (ie. using sacrificial initiators or detaching the grafted polymers) to directly evaluate the DP of grafted brush polymers and the surface density and the proportion of active initiators. Three high-density polymer brushes were grafted onto ATR silicon prisms and quantitative IR spectroscopy was used to monitor the grafting of ATRP initiators and compare the polymerization efficiency. Grafting densities of polymerization initiators ranged 0.9−1.7 molecules nm^{-2}. To obtain polymer brushes, the ATRP polymerization of styrene was then carried out without sacrificial initiators in the presence of $CuBr_2$ and a constant monomer concentration. Polymerization efficiency was assessed by measuring the areal concentration of polymerized styrene units. Obtained values fell in the range of 12−141 styrene units nm^{-2}. The lowest value corresponds to the grafting of polymerization initiators through amino linkers. The complexing affinity of these linkers with the reaction catalyst plausibly favors the dormant species at the expense of the active radical species in the ATRP process. In the absence of such an effect, polymerization is efficient and DP in the range of 200−1000 is obtained from the measurement of the polymer thickness and a scaling law (valid for a brush without solvent) relating it to DP. The efficiency of the grafted initiators is found to be in the range of 15−18%, independently of the initiator grafting density. In contrast, the polymerization kinetics are lowered by steric hindrance or conformational disorder in the layer of grafted initiators. The present approach of combining ATR-FTIR quantification together with AFM imaging to obtain a full characterization of polymer brushes is directly generalizable to any polymer system and any ATRP methods. It appears more relevant than classical methods based on the analysis of bulk polymers obtained by adding untethered initiators to the polymerization solution. It offers an alternative to the analysis of the brush swelling ratio and further provides the proportion of active initiators. We aim at using such a full characterization of such polymer brushes for applications in asymmetric catalysis.[54,74] Such a detailed characterization is of paramount importance to optimize the loading of active species and finely tune their further chemical reactions in a controlled way. Moreover, for the purpose of multicatalysis, the extension of the present method to copolymers is forecasted, notably to obtain information on the rate of incorporation of different monomer units. On this basis, a composition-property study can be seriously considered.

4. EXPERIMENTAL SECTION

4.1. Materials. All purchased chemicals were of reagent grade or higher (for all modifications on silicon substrate) and, if not mentioned explicitly, used without further purification. Undecylenic acid (99%) and undecylenic acid methyl ester (99%) were purchased from Acros Organics. 10-Undecen-1-ol (98%), *N*-(3-dimethylaminopropyl)-*N*′-ethylcarbodiimide (EDC, 98%), *N*-hydroxysuccinimide (NHS, commercial grade), ethyl 2-bromoisobutyrate (EBiB, 99%), α-bromoisobutyryl bromide (98%), *N*,*N*,*N*′,*N*″,*N*″-pentamethyldiethylenetriamine (98%) (PMDETA), Bipy (2,2′-bipyridyl, 99%), pyridine, copper(II), and copper(I) bromide (98%), and styrene (99%) were purchased from Sigma-Aldrich. The cleaning reagents [hydrogen peroxide 30%, sulfuric acid 96%, glacial acetic acid, tetrahydrofuran (THF), dichloromethane (DCM), acetonitrile (ACN)] and the etching reagent (hydrofluoric acid, HF, 50%) were of RSE quality and supplied by Carlo Erba. Diethylether was distilled over $LiAlH_4$, methanol was distilled from Mg, THF was distilled from sodium/benzophenone, and dichloromethane and hexane were distilled from CaH_2 before use. Molecular sieves 4 Å used in reaction were dried overnight at 500 °C then placed in a Schlenk tube under argon. Copper(I) bromide (CuBr, 98%) was purified with glacial acetic acid, washed with ethanol and diethylether, and stored under argon. Styrene was passed through a basic alumina gel column to remove traces of inhibitor. Ultrapure water UPW (Milli-Q, 18.2 MΩ•cm, at 25 °C) was used to prepare aqueous solutions and for rinsing. The silicon samples were cleaved from double-side-polished n-type silicon ((111), FZ, 30-40 Ωcm, Siltronix, France). They were glued with wax between two 45° machined aluminum blocks (see the Supporting Information, SI for more details), then both sample edges were mechanically polished with carborundum abrasive paper (from grit 240 to 1200). In a last step, both faces were polished with diamond paste of decreasing grain sizes (3 and 1 μm) until shining bevels are obtained. Each prism is accurately measured for the quantitative analysis. The typical size of a silicon prism is 20 × 13 × 0.5 mm and a bevel angle of 46°, giving ∼25 reflections.[45]

4.2. Syntheses of Initiators. *4.2.1. Initiator 1: N-(2-Aminoethyl)-2-bromo-2-methylpropanamide Hydrochloride.* The initiator is obtained in three steps: (1) Synthesis of *tert*-butyl (2-aminoethyl)-carbamate: A solution of di-*tert*-butyl dicarbonate (5.45 g, 25 mmol) in 1,4-dioxane (7 mL) was added dropwise into a solution of ethylenediamine (5 mL, 74.8 mmol) in 1,4-dioxane (50 mL). The solution was stirred at room temperature for 17 h. A white precipitate was filtered and the solution was concentrated under reduced pressure. The solid was solubilized in water (110 mL) and the white precipitate was filtered off. The solution was saturated with NaCl and extracted with DCM (3 × 60 mL). The compound was isolated as a pale yellow oil (1.9 g, 48%). ^{1}H NMR (300 MHz, $CDCl_3$): δ = 1.35 (s, 9H, *t*Bu), 1.57 (s, 2H, $N\underline{H}_2$), 2.66 (t, J = 6.0 Hz, 2H, $C\underline{H}_2NH_2$), 3.04 (q, J = 6.0 Hz, 2H, $C\underline{H}_2NHBoc$), 5.45 (brs, 1H, $N\underline{H}$); (2) Synthesis of *tert*-butyl 2-(2-bromo-2-methylpropanamido)-ethylcarbamate: α-bromoisobutyryl bromide (1.8 mL, 14.6 mmol) was added dropwise to a cooled (0 °C) solution of *tert*-butyl-(2-aminoethyl)carbamate (1.57 g, 9.8 mmol) in CH_2Cl_2 (25 mL) and

https://doi.org/10.1021/acsapm.2c01632
ACS Appl. Polym. Mater. XXXX, XXX, XXX−XXX

triethylamine (5.8 mL). The reaction solution was stirred at room temperature overnight and then poured into crushed ice (100 mL). The compound was extracted with DCM (3 × 100 mL). The combined organic phases were washed with water, aqueous saturated $NaHCO_3$ solution, and water, dried over anhydrous $MgSO_4$, and concentrated by vacuum. The solid was purified by flash chromatography on silica gel with ethyl acetate/petroleum ether (1/2.5) as elution solvent and the product was isolated as an orange powder (2 g, 56%). ^{1}H NMR (250 MHz, $CDCl_3$): δ = 1.34 (s, 9H, *t*Bu), 1.86 (s, 6H, $BrC(C\underline{H}_3)_2$), 3.26 (m, 4H, $C\underline{H}_2C\underline{H}_2$), 5.42 (brs, 2H, N<u>H</u>); (3) Synthesis of *N*-(2-aminoethyl)-2-bromo-2-methylpropanamide hydrochloride: *tert*-butyl 2-(2-bromo-2-methylpropanamido)ethylcarbamate (330 mg, 1.07 mmol) was dissolved in a 1 M solution of HCl in ether (10 mL). The solution was stirred at room temperature overnight. The white precipitate was filtered off and washed with cold diethylether. The hydrochloride was afforded (150 mg, 57%) as a white powder. ^{1}H NMR (300 MHz, D_2O): δ = 1.86 (s, 6H, $BrC(C\underline{H}_3)_2$), 3.10 (m, 2H, $C\underline{H}_2NH_3^+$), 3.47 (m, 2H, $C\underline{H}_2NH$).

4.2.2. Initiator 3: 10-Undecen-1-yl-2-bromo-2-methylpropionate. 10-Undecen-1-yl-2-bromo-2-methylpropionate was synthesized from 10-undecen-1-ol (8.3 mL, 41 mmol in 41 mL of dry THF) cooled at 0 °C, by the addition of α-bromoisobutyryl bromide (5.1 mL, 41 mmol) and pyridine (3.5 mL, 43 mmol). The reaction mixture was stirred for 3 h under argon, then n-hexane (25 mL) was added to the reaction. The resulting solution was washed with HCl (2 M) (2 × 50 mL) and H_2O (2 × 50 mL) and dried over anhydrous Na_2SO_4. The solvent was removed under reduced pressure to give the product as a colorless liquid (13 g, 94%). ^{1}H NMR (250 MHz, $CDCl_3$): δ = 1.20-1.44 (m, 12H, CH_2); 1.62-1.75 (m, 2H, $C\underline{H}_2$-CH_2O); 1.94 (s, 6H, $BrC(C\underline{H}_3)_2$); 2.05 (q, *J* = 7,0 Hz, 2H, $C\underline{H}_2$-CH_2=C<u>H</u>); 4.17 (t, *J* = 9,0 Hz, 2H, $CH_2C\underline{H}_2O$); 4.9-5.05 (m, 2H, $C\underline{H}_2$=CH); 5.72-5.9 (m, 1H, CH_2=C<u>H</u>).

4.3. Silicon Surface Modifications. *4.3.1. Preparation of Hydrogenated Silicon Surfaces (SiH_x).* The silicon prism was cleaned in a piranha solution (1:3 H_2O_2/H_2SO_4) at 100 °C for at least 2 h. After thorough rinsing with UPW, the prism was immersed for 5 s in a poly(tetrafluoroethylene) (PTFE) beaker filled with a 50% hydrofluoric acid solution, then rinsed with UPW in a beaker for 5 s. The SiH_x surface was dried in a flow of N_2.

4.3.2. Photochemical Grafting of Acid- or Methyl Ester-Terminated Alkyl Monolayers on the SiH_x Surfaces. Undecylenic acid (UA) or 10-methyl undecenoate (MeU) was outgassed under argon in a Schlenk tube at 100 °C for 30 min and then cooled to room temperature. The freshly prepared SiH_x prism was then transferred into the Schlenk tube with continuous argon bubbling for 15 min. The Schlenk was hermetically closed and irradiated for 3 h in a UV reactor (6 mW·cm^{-2}, 312 nm). The functionalized acid-terminated surface (Si-acid) was cleaned twice with glacial acetic acid under argon bubbling at 75 °C for 15 min in a Schlenk tube and, finally dried under N_2. For the ester-terminated surface (Si-ester), the prism was washed thoroughly with copious amounts of acetone to remove the residual ω-unsaturated alkyl ester and dried under N_2.

4.3.3. Activation of Si-Acid with EDC/NHS. Two solutions of 10 mM EDC and NHS were separately prepared in UPW at 4 °C. A Schlenk tube was immersed in a water bath with a temperature between 15 and 18 °C. An equal volume (5 mL) of EDC and NHS was added into the Schlenk tube and flushed with argon for 10 min before adding the acid-terminated silicon surface (Si-acid). For 90 min, the Schlenk tube with the prism was bubbled with argon, while the temperature was controlled to be maintained in the range mentioned above. Next, the prism Si-ester NHS was cleaned for 5 min in a beaker with UPW, then rinsed copiously with UPW, and dried under N_2.

4.3.4. Aminolysis of Initiator 1 on Si-Ester NHS. A fresh solution of initiator *N*-(2-aminoethyl)-2-bromo-2-methylpropanamide hydrochloride at a concentration of 20 mM in UPW was prepared; the pH was adjusted to 8.5−9 with 0.1 M NaOH solution. The solution was then bubbled in a Schlenk tube with argon for 5 min before the freshly activated prism was added. The argon bubbling was continued for 10 more minutes before the valves of the Schlenk were closed. After 3 h, the prism was cleaned for 2 min with THF and 2 min with DCM followed by a final short rinse in UPW before drying the prism Si-Br1 under a flow of N_2.

4.3.5. Reduction of Si-Ester with $LiAlH_4$. Diethylether (100 mL) was added to a dried Schlenk tube, previously purged with argon. About 5 g of $LiAlH_4$ powder was added slowly into the tube under stirring. The Si-ester prism was then immersed in the solution. The reaction mixture was kept at room temperature for 2 h. The modified prism was taken out from the reaction mixture and washed thoroughly with acetone, 0.5 M HCl solution, acetone, and UPW, sequentially. The prism Si-OH was then dried by pumping under reduced pressure for about 10 h and also at 80 °C under reduced pressure.

4.3.6. Esterification of Si-OH with α-Bromoisobutyryl Bromide. The prism Si-OH was placed in a solution of 1.5 mL of pyridine in 50 mL of dry diethylether, followed by dropwise addition of 2 mL of α-bromoisobutyryl bromide in 30 mL of dry diethylether over a period of 30 min. The reaction mixture was gently stirred at 0 °C for 2 h and then at room temperature overnight. The prism was taken out and washed with ethanol and water followed by a Soxhlet in DCM overnight. The prism Si-Br2 was then dried under N_2.

4.3.7. Grafting of Initiator 3 (10-Undecen-1-yl-2-bromo-2-methylpropionate) on Silicon Surface. The freshly HF-etched silicon prism was transferred into the Schlenk containing neat 10-undecen-1-yl-2-bromo-2-methylpropionate, previously bubbled with argon in a Schlenk tube for 30 min. Bubbling was maintained for 15 min. The Schlenk is hermetically closed and heated at 180 °C overnight. After the reaction, the prism Si-Br3 was washed ultrasonically with CH_2Cl_2, anhydrous ethyl alcohol, and UPW sequentially, each with 60 mL of solution for 3 min, respectively, and dried N_2.

4.3.8. Surface-Initiated Polymerization of Styrene on Silicon Surface. Polymerizations were performed using a mix of (monomer)/(CuBr)/($CuBr_2$)(PMDETA) = 100/1/0.05/1.2 molar ratio in a Schlenk tube at 100 °C. In a typical experiment for the preparation of PS brushes, the following amounts were used: styrene (4.36 mL, 38 mmol, 100 equiv), PMDETA (91 μL, 1.2 equiv), CuBr (55 mg, 1 equiv), and $CuBr_2$ (4.25 mg, 5 mol %), then the initiator-modified surface (Si-Br) was immersed in the medium, and the solution was degassed (three freeze−pump−thaw cycles) and back-filled with argon, and the reaction was allowed to proceed for 17 h at 100 °C. After polymerization, the silicon prism was purified by multiple washings with toluene, acetonitrile, and CH_2Cl_2, and a Soxhlet was carried out for 24 h in dichloromethane, then the prism was dried under nitrogen.

4.4. Instrumentation. *4.4.1. Nuclear Magnetic Resonance (NMR).* ^{1}H NMR spectra were recorded on a Bruker (AM 250 or 300 MHz) instrument with samples dissolved in $CDCl_3$. Chemical shifts (δ) are given in parts per million (ppm) with the signal of the residual $CHCl_3$ of the solvent as reference (7.24 ppm for ^{1}H NMR). The following abbreviations were used to describe the multiplicities: s (singlet), d (doublet), t (triplet), q (quadruplet), quint (quintet), m (multiplet), brs (broad singlet). All multiplicities were approximated to the first order; coupling constants, *J*, are reported in hertz and with an accuracy of 0.5 unit of the last digit.

4.4.2. Fourier Transform Infrared Spectroscopy in Attenuated Total Reflection (ATR-FTIR). The ATR-FTIR spectra are recorded on a Bruker Equinox FTIR spectrometer, coupled to a nitrogen-purged external ATR compartment, including a liquid-nitrogen-cooled MCT detector. All spectra are recorded in s- and p-polarization in the spectral range of 900−4000 cm^{-1} (150 scans, 4 cm^{-1} resolution). The spectra are presented in absorbance (computed using natural logarithm) and are normalized to the reflection number (around 26). The reference spectra are that of the hydrogenated SiHx surfaces. The calibration was performed in a homemade PTFCE IR cell of ∼2 mL volume. On the top and the bottom of the cell, a PTFE tube (0.8 mm diameter) is connected allowing for the addition of different solutions without breaking the spectrometer purge. On the side, there is a 9 mm diameter opening against which the Si prism (sample) is pressed via a nitrile O-ring seal.

https://doi.org/10.1021/acsapm.2c01632
ACS Appl. Polym. Mater. XXXX, XXX, XXX−XXX

4.4.3. X-ray Photoelectron Spectroscopy (XPS). These measurements were performed on a K-Alpha spectrometer from Thermo Fisher, equipped with a monochromatic X-ray Source (Al Kα, 1486.6 eV). For all measurements, a spot size of 400 mm was employed. The hemispherical analyzer was operated in CAE (Constant Analyzer Energy) mode, with a pass energy of 200 eV and a step of 1 eV for the acquisition of surveys spectra, and a pass energy of 50 eV and a step of 0.1 eV for the acquisition of high-resolution spectra. A "dual-beam" flood gun was used to neutralize the charge buildup. The recorded spectra were processed by means of Avantage software provided by Thermo Fisher using a peak fitting routine with Shirley background and symmetrical Gaussian−Lorentzian lineshapes. The quantification was performed after normalization of the peak areas with Scofield sensitivity factors. The calibration in binding energy was made by considering that the Csp3 component of C 1s lies at 285 eV.

4.4.4. Contact Angle. Static contact angle measurement was performed using a DSA100 Kruss analyzer. The water contact angle was measured by depositing a 3 μL droplet of UPW on the surface, the average contact angle was calculated from three droplets for each surface, and errors were calculated as standard deviation.

4.4.5. Atomic Force Microscopy. Images were recorded under N_2 atmosphere using AFM operating in AC-mode (PicoSPM 5500, Agilent) and silicon tips (HQ-NSC16S cantilevers from Mikro-Masch). To measure the thickness of the organic layers, part of the layer was locally removed by scratching using a syringe needle. The layer thickness was deduced from cross sections and histograms of the height distribution on images captured at the frontier between the bare silicon (inside the scratch) and the top of the organic layer.

4.4.6. Ellipsometry. Thickness measurements were carried out using an Accurion nanofilm EP3 ellipsometer. The thickness is obtained by measuring the change in the polarization of light (at fixed λ = 658 nm) as it is reflected off the surface over a range of angles (from 50 to 75° with 1 step number). Thicknesses are obtained with an accuracy of up to a fraction of nanometer.

■ ASSOCIATED CONTENT

Supporting Information

The Supporting Information is available free of charge at https://pubs.acs.org/doi/10.1021/acsapm.2c01632.

IR quantification of the chemical groups on crystalline Si (SI-I); surface characterization of grafted initiators (SI-II); and calibration of the polystyrene IR absorption (SI-III) (PDF)

■ AUTHOR INFORMATION

Corresponding Authors

Anne-Chantal Gouget-Laemmel − *Laboratoire de Physique de la Matière Condensée, CNRS, Ecole Polytechnique, Institut Polytechnique de Paris, 91120 Palaiseau, France;* orcid.org/0000-0002-7477-9200; Email: anne-chantal.gouget@polytechnique.edu

Philippe Roger − *Institut de Chimie Moléculaire et des Matériaux d'Orsay, Université Paris-Saclay, CNRS, 91405 Orsay, France;* orcid.org/0000-0001-9811-4580; Email: philippe.roger@universite-paris-saclay.fr

Authors

Nacim Zidelmal − *Institut de Chimie Moléculaire et des Matériaux d'Orsay, Université Paris-Saclay, CNRS, 91405 Orsay, France*

Rafaela S. B. Soares − *Laboratoire de Physique de la Matière Condensée, CNRS, Ecole Polytechnique, Institut Polytechnique de Paris, 91120 Palaiseau, France;* orcid.org/0000-0002-0473-8454

Nadine Barroca-Aubry − *Institut de Chimie Moléculaire et des Matériaux d'Orsay, Université Paris-Saclay, CNRS, 91405 Orsay, France;* orcid.org/0000-0003-0695-8255

Diana Dragoe − *Institut de Chimie Moléculaire et des Matériaux d'Orsay, Université Paris-Saclay, CNRS, 91405 Orsay, France;* orcid.org/0000-0002-8536-1205

Ludovic Costa − *Institut de Chimie Moléculaire et des Matériaux d'Orsay, Université Paris-Saclay, CNRS, 91405 Orsay, France;* orcid.org/0000-0001-8041-4382

Bénédicte Lepoittevin − *Laboratoire de Chimie Moléculaire et Thio-organique (LCMT), Normandie Univ, ENSICAEN, UNICAEN, CNRS, 14000 Caen, France;* orcid.org/0000-0002-2210-2337

Hanène Salmi-Mani − *Institut de Chimie Moléculaire et des Matériaux d'Orsay, Université Paris-Saclay, CNRS, 91405 Orsay, France;* orcid.org/0000-0002-3464-1100

Mohamed Mellah − *Institut de Chimie Moléculaire et des Matériaux d'Orsay, Université Paris-Saclay, CNRS, 91405 Orsay, France;* orcid.org/0000-0002-8006-8149

Catherine Henry-de-Villeneuve − *Laboratoire de Physique de la Matière Condensée, CNRS, Ecole Polytechnique, Institut Polytechnique de Paris, 91120 Palaiseau, France;* orcid.org/0000-0002-8668-3070

François Ozanam − *Laboratoire de Physique de la Matière Condensée, CNRS, Ecole Polytechnique, Institut Polytechnique de Paris, 91120 Palaiseau, France;* orcid.org/0000-0003-0002-8372

Emmanuelle Schulz − *Institut de Chimie Moléculaire et des Matériaux d'Orsay, Université Paris-Saclay, CNRS, 91405 Orsay, France;* orcid.org/0000-0002-0844-8825

Complete contact information is available at: https://pubs.acs.org/10.1021/acsapm.2c01632

Notes

The authors declare no competing financial interest.

The authors declare that they have no known competing financial interests or personal relationships that could have appeared to influence the work reported in this paper.

■ ACKNOWLEDGMENTS

The authors thank the French National Research Agency (Charmmmat ANR-11-LABX-0039) for financial support and PhD fellowship to N.Z.

■ REFERENCES

(1) Rasouli, R.; Barhoum, A.; Uludag, H. A Review of Nanostructured Surfaces and Materials for Dental Implants: Surface Coating, Patterning and Functionalization for Improved Performance. *Biomater. Sci.* **2018**, *6*, 1312−1338.

(2) Kumari, S.; Tiyyagura, H. R.; Pottathara, Y. B.; Sadasivuni, K. K.; Ponnamma, D.; Douglas, T. E. L.; Skirtach, A. G.; Mohan, M. K. Surface Functionalization of Chitosan as a Coating Material for Orthopaedic Applications: A Comprehensive Review. *Carbohydr. Polym.* **2021**, *255*, No. 117487.

(3) Wieszczycka, K.; Staszak, K.; Wozniak-Budych, M. J.; Litowczenko, J.; Maciejewska, B. M.; Jurga, S. Surface Functionalization—The Way for Advanced Applications of Smart Materials. *Coord. Chem. Rev.* **2021**, *436*, No. 213846.

(4) Liu, J.; Yao, Y.; Li, X. H.; Zhang, Z. J. Fabrication of Advanced Polydimethylsiloxane-based Functional Materials: Bulk Modifications and Surface Functionalizations. *Chem. Eng. J.* **2021**, *408*, No. 127612.

(5) Long, W.; Ouyang, H.; Hu, X.; Liu, M. Y.; Zhang, X. Y.; Feng, Y. L.; Wei, Y. State-of-Art Review on Preparation, Surface Functionaliza-

tion and Biomedical Applications of Cellulose Nanocrystals-based Materials. *Int. J. Biol. Macromol.* **2021**, *186*, 591−615.
(6) Azzaroni, O. Polymer Brushes Here, There, and Everywhere: Recent Advances in their Practical Applications and Emerging Opportunities in Multiple Research Fields. *J. Polym. Sci., Part A: Polym. Chem.* **2012**, *50*, 3225−3258.
(7) Zoppe, J. O.; Ataman, N. C.; Mocny, P.; Wang, J.; Moraes, J.; Klok, H. A. Surface-Initiated Controlled Radical Polymerization: State-of-the-Art, Opportunities, and Challenges in Surface and Interface Engineering with Polymer Brushes. *Chem. Rev.* **2017**, *117*, 1105−1318.
(8) Ma, S. H.; Zhang, X. Q.; Yu, B.; Zhou, F. Brushing Up Functional Materials. *NPG Asia Mater.* **2019**, *11*, 24.
(9) Nasef, M. M.; Gupta, B.; Shameli, K.; Verma, C.; Ali, R. R.; Ting, T. M. Engineered Bioactive Polymeric Surfaces by Radiation Induced Graft Copolymerization: Strategies and Applications. *Polymers* **2021**, *13*, 3102.
(10) Bedel, S.; Lepoittevin, B.; Costa, L.; Leroy, O.; Dragoe, D.; Bruzaud, J.; Herry, J. M.; Guilbaud, M.; Bellon-Fontaine, M. N.; Roger, P. Antibacterial Poly(thylene terephthalate) Surfaces Obtained from Thymyl Methacrylate Polymerization. *J. Polym. Sci., Part A: Polym. Chem.* **2015**, *53*, 1975−1985.
(11) Anjum, S.; Singh, S.; Lepoittevin, B.; Roger, P.; Panigrahi, M.; Gupta, B. Biomodification Strategies for the Development of Antimicrobial Urinary Catheters: Overview and Advances. *Global Challenges* **2017**, *2*, No. 1700068.
(12) Edwards, J. V.; Vigo, T. L. *Bioactive Fibers and Polymers*, ACS Symposium Series; Springer, 2001; p 792.
(13) Lejars, M.; Margaillan, A.; Bressy, C. Fouling Release Coatings: A Nontoxic Alternative to Biocidal Antifouling Coatings. *Chem. Rev.* **2012**, *112*, 4347−4390.
(14) Gautam, B.; Yu, H. H. Self-Cleaning Cotton Obtained after Grafting Thermoresponsive Poly(N-vinylcaprolactam) through Surface-Initiated Atom Transfer Radical Polymerization. *Polymers* **2020**, *12*, 2920.
(15) Zhu, Z. Y.; Huang, Z. N.; Huang, W.; Wen, H.; Zhang, J. Y.; Wang, P.; Peng, Y.; Liu, C. K. Polymer Brush-Grafted Cotton Fiber for the Efficient Removal of Aromatic Halogenated Disinfection By-products in Drinking Water. *J. Colloid Interface Sci.* **2021**, *597*, 66−74.
(16) Hyder, M. K. M. Z.; Ochiai, B. Synthesis of a Highly Selective Scavenger of Precious Metals from a Printed Circuit Board Based on Cellulose Filter Paper Functionalized with a Grafted Polymer Chain Bearing N-Methyl-2-hydroxyethylcarbamothioate Moieties. *ACS Omega* **2022**, *7*, 10355−10364.
(17) Wei, Q. B.; Cai, M. R.; Zhou, F.; Liu, W. M. Dramatically Tuning Friction Using Responsive Polyelectrolyte Brushes. *Macromolecules* **2013**, *46*, 9368−9379.
(18) Wang, S. G.; Wang, Z. W.; Li, J.; Li, L. Q.; Hu, W. P. Surface-grafting Polymers: from Chemistry to Organic Electronics. *Mater. Chem. Front.* **2020**, *4*, 692−714.
(19) Gill, C. S.; Long, W.; Jones, C. W. Magnetic Nanoparticle Polymer Brush Catalysts: Alternative Hybrid Organic/Inorganic Structures to Obtain High, Local Catalyst Loadings for Use in Organic Transformations. *Catal. Lett.* **2009**, *131*, 425−431.
(20) Zhao, B.; Brittain, W. J. Polymer Brushes: Surface-Immobilized Macromolecules. *Progr. Polym. Sci.* **2000**, *25*, 677−710.
(21) Tsujii, Y.; Ohno, K.; Yamamoto, S.; Goto, A.; Fukuda, T. Structure and Properties of High-Density Polymer Brushes Prepared by Surface-Initiated Living Radical Polymerization. In *Surface-Initiated Polymerization I. Advances in Polymer Science*, Jordan, R., Ed.; Springer: Berlin, Heidelberg, 2006; Vol. *197*, pp 1−45.
(22) Yamamoto, S.; Ejaz, M.; Tsujii, Y.; Matsumoto, M.; Fukuda, T. Surface Interaction Forces of Well-Defined, High-Density Polymer Brushes Studied by Atomic Force Microscopy. 1. Effect of Chain Length. *Macromolecules* **2000**, *33*, 5602−5607.
(23) Yamamoto, S.; Ejaz, M.; Tsujii, Y.; Fukuda, T. Surface Interaction Forces of Well-Defined, High-Density Polymer Brushes Studied by Atomic Force Microscopy. 2. Effect of Graft Density. *Macromolecules* **2000**, *33*, 5608−5612.
(24) Flejszar, M.; Chmielarz, P. Surface-Initiated Atom Transfer Radical Polymerization for the Preparation of Well-Defined Organic-Inorganic Hybrid Nanomaterials. *Materials* **2019**, *12*, 3030.
(25) Pyun, J.; Kowalewski, T.; Matyjaszewski, K. Synthesis of Polymer Brushes Using Atom Transfer Radical Polymerization. *Macromol. Rapid Commun.* **2003**, *24*, 1043−1059.
(26) Gao, H. F.; Matyjaszewski, K. Synthesis of Star Polymers by a Combination of ATRP and the ″Click″ Coupling Method. *Macromolecules* **2006**, *39*, 4960−4965.
(27) Matyjaszewski, K.; Miller, P. J.; Shukla, N.; Immaraporn, B.; Gelman, A.; Luokala, B. B.; Siclovan, T. M.; Kickelbick, G.; Vallant, T.; Hoffmann, H.; Pakula, T. Polymers at Interfaces: Using Atom Transfer Radical Polymerization in the Controlled Growth of Homopolymers and Block Copolymers from Silicon surfaces in the Absence of Untethered Sacrificial Initiator. *Macromolecules* **1999**, *32*, 8716−8724.
(28) Ejaz, M.; Yamamoto, S.; Ohno, K.; Tsujii, Y.; Fukuda, T. Controlled Graft Polymerization of Methyl Methacrylate on Silicon Substrate by the Combined Use of the Langmuir-Blodgett and Atom Transfer Radical Polymerization Techniques. *Macromolecules* **1998**, *31*, 5934−5936.
(29) Zaborniak, I.; Chmielarz, P.; Wolski, K. Riboflavin-Induced Metal-Free ATRP of (Meth)acrylates. *Eur. Polym. J.* **2020**, *140*, No. 110055.
(30) Zaborniak, I.; Chmielarz, P.; Matyjaszewski, K. Synthesis of Riboflavin-Based Macromolecules through Low ppm ATRP in Aqueous Media. *Macromol. Chem. Phys.* **2020**, *221*, No. 1900496.
(31) Pan, X.; Fantin, M.; Yuan, F.; Matyjaszewski, K. Externally Controlled Atom Transfer Radical Polymerization. *Chem. Soc. Rev.* **2018**, *47*, 5457−5490.
(32) Li, D.; Niu, X. Q.; Yang, S. Y.; Chen, Y. H.; Ran, F. Thermo-Responsive Polysulfone Membranes with Good Anti-Fouling Property Modified by Grafting Random Copolymers via Surface-Initiated eATRP. *Sep. Purif. Technol.* **2018**, *206*, 166−176.
(33) Strover, L. T.; Malmstrom, J.; Stubbing, L. A.; Brimble, M. A.; Travas-Sejdic, J. Electrochemically-Controlled Grafting of Hydrophilic Brushes from Conducting Polymer Substrates. *Electrochim. Acta* **2016**, *188*, 57−70.
(34) Chmielarz, P.; Krys, P.; Park, S.; Matyjaszewski, K. PEO-b-PNIPAM Copolymers via SARA ATRP and eATRP in Aqueous Media. *Polymer* **2015**, *71*, 143−147.
(35) Dadashi-Silab, S.; Doran, S.; Yagci, Y. Photoinduced Electron Transfer Reactions for Macromolecular Syntheses. *Chem. Rev.* **2016**, *116*, 10212−10275.
(36) Razeghi, R.; Kazemi, F.; Nikfarjam, N.; Shariati, Y.; Kaboudin, B. Visible Photo-Induced Catalyst-Free Polymerization via In Situ Prepared Dibromide. *Eur. Polym. J.* **2021**, *144*, No. 110195.
(37) Fors, B. P.; Hawker, C. J. Control of a Living Radical Polymerization of Methacrylates by Light. *Angew. Chem., Int. Ed.* **2012**, *51*, 8850−8853.
(38) Jordan, R.; Ulman, A.; Kang, J. F.; Rafailovich, M. H.; Sokolov, J. Surface-Initiated Anionic Polymerization of Styrene by Means of Self-Assembled Monolayers. *J. Am. Chem. Soc.* **1999**, *121*, 1016−1022.
(39) Wang, S. Q.; Zhu, Y. X. Facile Method to Prepare Smooth and Homogeneous Polymer Brush Surfaces of Varied Brush Thickness and Grafting Density. *Langmuir* **2009**, *25*, 13448−13455.
(40) Słowikowska, M.; Chajec, K.; Michalski, A.; Zapotoczny, S.; Wolski, K. Surface-Initiated Photoinduced Iron-Catalyzed Atom Transfer Radical Polymerization with ppm Concentration of FeBr3 under Visible Light. *Materials* **2020**, *13*, 5139.
(41) Bech, L.; Elzein, T.; Meylheuc, T.; Ponche, A.; Brogly, M.; Lepoittevin, B.; Roger, P. Atom Transfer Radical Polymerization of Styrene from Different Poly(ethylene terephthalate) Surfaces: Films, Fibers and Fabrics. *Eur. Polym. J.* **2009**, *45*, 246−255.
(42) Boukherroub, R.; Morin, S.; Bensebaa, F.; Wayner, D. D. M. New Synthetic Routes to Alkyl Monolayers on the Si(111) Surface. *Langmuir* **1999**, *15*, 3831−3835.
(43) Jakob, P.; Chabal, Y. J. Chemcial Etching of Vicinal Si(111)—Dependence of the Surface-Structure and the Hydrogen Termination

https://doi.org/10.1021/acsapm.2c01632
ACS Appl. Polym. Mater. XXXX, XXX, XXX−XXX

on the pH of the Etching Solutions. *J. Chem. Phys.* **1991**, *95*, 2897−2909.
(44) Karimi, M.; Tashvigh, A. A.; Asadi, F.; Ashtiani, F. Z. Determination of Concentration-Dependent Diffusion Coefficient of Seven Solvents in Polystyrene Systems using FTIR-ATR Technique: Experimental and Mathematical Studies. *RSC Adv.* **2016**, *6*, 9013−9022.
(45) Ozanam, F.; Chazalviel, J. N. Fourier-Transform Electrochemically Modulated Infrared-Spectroscopy. *J. Electron Spectrosc. Relat. Phenom.* **1987**, *45*, 323−334.
(46) Bélanger, D.; Pinson, J. Electrografting: A Powerful Method for Surface Modification. *Chem. Soc. Rev.* **2011**, *40*, 3995−4048.
(47) Fabre, B. Functionalization of Oxide-Free Silicon Surfaces with Redox-Active Assemblies. *Chem. Rev.* **2016**, *116*, 4808−4849.
(48) Gooding, J. J.; Ciampi, S. The Molecular Level Modification of Surfaces: From Self-Assembled Monolayers to Complex Molecular Assemblies. *Chem. Soc. Rev.* **2011**, *40*, 2704−2718.
(49) Chabal, Y. J. Surface Infrared-Spectroscopy. *Surf. Sci. Rep.* **1988**, *8*, 211−357.
(50) Faucheux, A.; Gouget-Laemmel, A. C.; Henry de Villeneuve, C.; Boukherroub, R.; Ozanam, F.; Allongue, P.; Chazalviel, J.-N. Well-Defined Carboxyl-Terminated Alkyl Monolayers Grafted onto H-Si(111): Packing Density from a Combined AFM and Quantitative IR Study. *Langmuir* **2006**, *22*, 153−162.
(51) Aschl, T.; Frison, G.; Moraillon, A.; Ozanam, F.; Allongue, P.; Gouget-Laemmel, A. C. Insights into the Ochratoxin A/Aptamer Interactions on a Functionalized Silicon Surface by Fourier Transform Infrared and UV-Vis Studies. *Langmuir* **2020**, *36*, 13908−13917.
(52) Francis, R.; Lepoittevin, B.; Taton, D.; Gnanou, Y. Toward an Easy Access to Asymmetric Stars and Miktoarm Stars by Atom Transfer Radical Polymerization. *Macromolecules* **2002**, *35*, 9001−9008.
(53) Xia, J. H.; Matyjaszewski, K. Controlled/"Living" Radical Polymerization. Atom Transfer Radical Polymerization Using Multidentate Amine Ligands. *Macromolecules* **1997**, *30*, 7697−7700.
(54) Zidelmal, N.; Aubry-Barroca, N.; Lepoittevin, B.; Mellah, M.; Costa, L.; Ozanam, F.; Gouget-Laemmel, A. C.; Schulz, E.; Roger, P. Synthesis, Characterization and Catalytic Properties of Salen-Containing Polymers Obtained by Atom Transfer Radical Polymerization. *Polymer* **2018**, *135*, 261−270.
(55) Sam, S.; Touahir, L.; Salvador Andresa, J.; Allongue, P.; Chazalviel, J.-N.; Gouget-Laemmel, A. C.; Henry de Villeneuve, C.; Moraillon, A.; Ozanam, F.; Gabouze, N.; Djebbar, S. Semiquantitative Study of the EDC/NHS Activation of Acid Terminal Groups at Modified Porous Silicon Surfaces. *Langmuir* **2010**, *26*, 809−814.
(56) Palazon, F.; Benavides, C. M.; Leonard, D.; Souteyrand, E.; Chevolot, Y.; Cloarec, J. P. Carbodiimide/NHS Derivatization of COOH-Terminated SAMs: Activation or Byproduct Formation? *Langmuir* **2014**, *30*, 4545−4550.
(57) Zhang, C.; Luo, N.; Hirt, D. E. Surface Grafting Polyethylene glycol (PEG) onto Poly(ethylene-co-acrylic acid) films. *Langmuir* **2006**, *22*, 6851−6857.
(58) Oliverio, M.; Perotto, S.; Messina, G. C.; Lovato, L.; De Angelis, F. Chemical Functionalization of Plasmonic Surface Biosensors: A Tutorial Review on Issues, Strategies, and Costs. *ACS Appl. Mater. Interfaces* **2017**, *9*, 29394−29411.
(59) Lepoittevin, B.; Costa, L.; Pardoue, S.; Dragoe, D.; Mazerat, S.; Roger, P. Hydrophilic PET Surfaces by Aminolysis and Glycopolymer Brushes Chemistry. *J. Polym. Sci., Part A: Polym. Chem.* **2016**, *54*, 2689−2697.
(60) Xu, Y.; Sui, X.; Guan, S.; Zhai, J.; Gao, L. Olfactory Sensory Neuron-Mimetic CO2 Activated Nanofluidic Diode with Fast Response Rate. *Adv. Mater.* **2015**, *27*, 1851−1855.
(61) Moraillon, A.; Gouget-Laemmel, A. C.; Ozanam, F.; Chazalviel, J.-N. Amidation of Monolayers on Silicon in Physiological Buffers: A Quantitative IR Study. *J. Phys. Chem. C* **2008**, *112*, 7158−7167.
(62) Sieval, A. B.; van den Hout, B.; Zuilhof, H.; Sudhölter, E. J. R. Molecular Modeling of Alkyl Monolayers on the Si(111) Surface. *Langmuir* **2000**, *16*, 2987−2990.
(63) Wang, Z.; Zuilhof, H. Self-Healing Fluoropolymer Brushes as Highly Polymer-Repellent Coatings. *J. Mater. Chem. A* **2016**, *4*, 2408−2412.
(64) Yu, W. H.; Kang, E. T.; Neoh, K. G.; Zhu, S. P. Controlled Grafting of Well-Defined Polymers on Hydrogen-Terminated Silicon Substrates by Surface-Initiated Atom Transfer Radical olymerization. *J. Phys. Chem. B* **2003**, *107*, 10198−10205.
(65) Yang, Q.; Tian, J.; Hu, M.-X.; Xu, Z.-K. Construction of a Comb-Like Glycosylated Membrane Surface by a Combination of UV-Induced Graft Polymerization and Surface-Initiated ATRP. *Langmuir* **2007**, *23*, 6684−6690.
(66) Bozukova, D.; Pagnoulle, C.; De Pauw-Gillet, M.-C.; Ruth, N.; Jerome, R.; Jerome, C. Imparting Antifouling Properties of Poly(2-hydroxyethyl methacrylate) Hydrogels by Grafting Poly(oligoethylene glycol methyl ether acrylate). *Langmuir* **2008**, *24*, 6649−6658.
(67) daFonseca, C.; Ozanam, F.; Chazalviel, J. N. In Situ Infrared Characterisation of the Interfacial Oxide During the Anodic Dissolution of a Silicon Electrode in Fluoride Electrolytes. *Surf. Sci.* **1996**, *365*, 1−14.
(68) Wallart, X.; de Villeneuve, C. H.; Allongue, P. Truly Quantitative XPS Characterization of Organic Monolayers on Silicon: Study of Alkyl and Alkoxy Monolayers on H-Si(111). *J. Am. Chem. Soc.* **2005**, *127*, 7871−7878.
(69) Al-Bataineh, S. A.; Britcher, L. G.; Griesser, H. J. Rapid Radiation Degradation in the XPS Analysis of Antibacterial Coatings of Brominated Furanones. *Surf. Interface Anal.* **2006**, *38*, 1512−1518.
(70) Bedel, S.; Lepoittevin, B.; Costa, L.; Leroy, O.; Dragoe, D.; Bruzaud, J.; Herry, J.-M.; Guilbaud, M.; Bellon-Fontaine, M.-N.; Roger, P. Antibacterial Poly(ethylene terephthalate) Surfaces Obtained from Thymyl Methacrylate Polymerization. *J. Polym. Sci., Part A: Polym. Chem.* **2015**, *53*, 1975−1985.
(71) Liang, C. Y.; Krimm, S. Infrared Spectra of High Polymers. 6. Polystyrene. *J. Polym. Sci.* **1958**, *27*, 241−254.
(72) Neppel, A.; Butler, I. S. Infrared and Raman-Spectra of Poly(alpha-methyl styrene). *Spectrochim. Acta, Part A* **1984**, *40*, 1095−1100.
(73) Hinode, K.; Takeda, K.; Kondo, S. Abnormal Room-Temperature Oxidation of Silicon in the Presence of Copper. *J. Vac. Sci. Technol., A* **2002**, *20*, 1653−1658.
(74) Bakangura, E.; Roger, P.; Soares, R. S. B.; Mellah, M.; Barroca-Aubry, N.; Gouget-Laemmel, A. C.; Ozanam, F.; Costa, L.; Baltaze, J. P.; Schulz, E. Post-Modification of Copolymers Obtained by ATRP for an Application in Heterogeneous Asymmetric Salen Catalysis. *Molecules* **2022**, *27*, 4654.

https://doi.org/10.1021/acsapm.2c01632
ACS Appl. Polym. Mater. XXXX, XXX, XXX−XXX